

This document is confidential and is proprietary to the American Chemical Society and its authors. Do not copy or disclose without written permission. If you have received this item in error, notify the sender and delete all copies.

Discovery of Diverse Natural Products as inhibitors of SARS-CoV-2 Mpro Protease through Virtual Screening

Journal:	<i>Journal of Chemical Information and Modeling</i>
Manuscript ID	ci-2021-00951c.R2
Manuscript Type:	Article
Date Submitted by the Author:	12-Nov-2021
Complete List of Authors:	Rubio Martinez, Jaime; Universitat de Barcelona, Departament de Ciència dels Materials i Química Física Jimenez-Alesanco, Ana ; University of Zaragoza Institute of Biocomputation and Physics of Complex Systems Ceballos-Laita, Laura; University of Zaragoza Institute of Biocomputation and Physics of Complex Systems, Ortega Alarcón, David; University of Zaragoza Institute of Biocomputation and Physics of Complex Systems Vega, Sonia; University of Zaragoza Institute of Biocomputation and Physics of Complex Systems Calvo, Cristina; Molecular Biology Institute of Barcelona Benitez, Cristina; Molecular Biology Institute of Barcelona Abián, Olga; Universidad de Zaragoza, Departamento de Bioquímica y Biología Velázquez-Campoy, Adrián; Universidad de Zaragoza, Instituto de Biocomputacion y Fisica de Sistemas Complejos Thomson, Timothy; Molecular Biology Institute of Barcelona; Universidad Peruana Cayetano Heredia Granadino-Roldan, Jose; Universidad de Jaen, Physical and Analytical Chemistry Gomez-Gutierrez, Patricia; Universitat Politecnica de Catalunya, Chemical Engineering Perez, Juan J.; Universitat Politecnica de Catalunya, enginyeria quimica

SCHOLARONE™
Manuscripts

Discovery of Diverse Natural Products as inhibitors of SARS-CoV-2 M^{pro} Protease through Virtual Screening

Jaime Rubio-Martínez^{1,*}, Ana Jiménez-Alesanco^{2,3}, Laura Ceballos-Laita^{2,4}, David Ortega-Alarcón^{2,3}, Sonia Vega², Cristina Calvo^{5,6}, Cristina Benítez^{5,6}, Olga Abian^{2,3,4,5,7}, Adrián Velázquez-Campoy^{2,3,4,5,8}, Timothy Thomson^{5,6,9}, José Manuel Granadino-Roldán¹⁰, Patricia Gómez-Gutiérrez¹¹, Juan J. Pérez¹¹.

¹Department of Materials Science and Physical Chemistry, University of Barcelona and the Institut de Recerca en Química Teòrica i Computacional (IQTCUB), 08028 Barcelona, Spain

²Institute for Biocomputation and Physics of Complex Systems (BIFI), Joint Units IQFR-CSIC-BIFI, and GBsC-CSIC-BIFI, Universidad de Zaragoza, 50018 Zaragoza, Spain

³Departamento de Bioquímica y Biología Molecular y Celular, Universidad de Zaragoza, 50009 Zaragoza, Spain

⁴Instituto de Investigación Sanitaria de Aragón (IIS Aragón), 50009 Zaragoza, Spain

⁵Centro de Investigación Biomédica en Red en el Área Temática de Enfermedades Hepáticas Digestivas (CIBERehd), 28029 Madrid, Spain

⁷Instituto Aragonés de Ciencias de la Salud (IACS), 50009 Zaragoza, Spain.

⁶Institute of Molecular Biology of Barcelona (IBMB-CSIC), 08028 Barcelona, Spain

⁸Fundación ARAID, Gobierno de Aragón, 50018 Zaragoza, Spain

⁹Universidad Peruana Cayetano Heredia, San Martín de Porres 15102, Perú.

¹⁰Departamento de Química Física y Analítica, Facultad de Ciencias Experimentales, Universidad de Jaén, Campus "Las Lagunillas" s/n, 23071, Jaén, Spain

¹¹Department of Chemical Engineering. Universitat Politècnica de Catalunya- Barcelona Tech. Av. Diagonal, 647. 08028 Barcelona, Spain

*Address for correspondence: Jaime Rubio-Martínez, Martí i Franques 1, E-08028 Barcelona, Spain. Phone: (+34) 93 4039263; Fax: (+34) 93 4021231; E-mail: jaime.rubio@ub.edu

Abstract

SARS-CoV-2 is a coronavirus responsible for the international outbreak of respiratory illness termed Covid-19 that forced the World Health Organization to declare a pandemic infectious disease situation of international concern at the beginning of 2020. The need for a swift response against Covid-19 prompted to consider different sources to identify bioactive compounds that can be used as therapeutical agents including available drugs and natural products. Accordingly, this work reports the results of a virtual screening process aimed at identifying antiviral natural products inhibitors of the SARS-CoV-2 M^{pro} viral protease. For this purpose, ca. 2000 compounds of the Selleck database of Natural Compounds were subject of an ensemble docking process targeting the M^{pro} protease. Molecules that showed binding to most of the protein conformations were retained for a further step that involved the computation of the binding free energy of the ligand-M^{pro} complex along a molecular dynamics trajectory. Those compounds showing a smooth binding free energy behaviour were selected for *in vitro* testing. From the resulting set of compounds, five exhibit an antiviral profile and are disclosed in the present work.

Introduction

Coronaviruses, like other members of the coronaviridae family are enveloped, positive single-stranded RNA viruses infecting a wide range of hosts including avian, swine and humans [1]. While most members of the family produce mild respiratory effects in humans, the 21st century has witnessed the appearance of new members producing severe respiratory diseases in afflicted individuals. SARS-CoV-1 was identified as the pathogen responsible for an outbreak of a severe acute respiratory syndrome (SARS) in the Guangdong Province, China in 2002, and 10 years later, MERS-CoV was identified in the sputum of a patient that was retrospectively diagnosed with the Middle East respiratory syndrome (MERS) in Jordania. Both pathogens produced an epidemic that spread into several countries due international travel of infected persons that ended about a year later of the outbreak after taking strict measures of infection control [2]. Beginning in December 2019, a novel coronavirus, designated as SARS-CoV-2 was identified as the pathogen causing an international outbreak of respiratory illness termed Covid-19, originated in Wuhan, Hubei Province, China. Data gathered on the epidemic suggests that although SARS-CoV-2 exhibits a ~2% fatality rate, lower than its two ancestors, it is more contagious resulting in higher overall death tolls. This fact forced the World Health Organization to declare SARS-CoV-2 as a pandemic infectious disease of international concern on March 11, 2020 [3]. Until June 20th, 2021, there are 178.491.800 confirmed cases of Covid-19 with 3.866.200 confirmed deaths worldwide [4].

The need for a swift response against Covid-19 prompted to consider drug repurposing as a valuable strategy to cope with the pandemic in a reasonable period of time [5]. Today, there are a few hundred on-going clinical trials aimed at assessing the effect of diverse available drugs at different stages of the disease [6]. A few drugs are currently available for the treatment of Covid-19 patients [7-9]. Specifically, remdesivir alone [10] or combined with the Janus kinase inhibitor baricitinib [11] is the only antiviral agent against SARS-CoV-2 approved with an emergency use authorization for the treatment of patients with severe symptoms. Other antivirals already marketed, like favipiravir [12] and EIDD-2801 [13] show mixed evidence whereas, drugs like lopinavir and ritonavir were shown

1
2
3 ineffective for the treatment of Covid-19 [14]. Similarly, the antimalarial
4 hydroxychloroquine and chloroquine were also shown ineffective [14,15]. Presently, clinical
5 treatment of Covid-19 is mainly symptomatic using anti-inflammatories like
6 dexamethasone [16] or cytokine inhibitors, combined with antibiotics to treat secondary
7 infections. Accordingly, there remains an urgent need for the development of specific
8 antiviral therapeutics against SARS-CoV-2.
9
10
11
12
13

14
15 Among the diverse targets available to design antiviral agents, the main proteinase
16 (M^{pro}) constitutes an attractive one, since it controls the activities of the coronavirus
17 replication complex. Inhibition of M^{pro} was demonstrated to be effective against SARS-CoV-
18 1 *in vitro* [17]. Accordingly, several recent studies focus on the design and discovery of
19 inhibitors of the M^{pro} protease for its use as antiviral agents for the treatment of Covid-19.
20 Thus, as a follow up of previous work devoted to design suicide inhibitors of M^{pro} in diverse
21 coronavirus, a α -ketoamide has been recently disclosed as a potent inhibitor of the SARS-
22 CoV-2 protease *in vitro* [18]. Other authors have also reported the design of non-covalent
23 inhibitors with a high inhibitory profile against virus duplication *in vitro* [19, 20]. In the
24 present study, we specifically focus in the identification of natural products, inhibitors of
25 M^{pro} for its use as antiviral agents for the treatment of Covid-19, through the use of virtual
26 screening. Natural products represent an interesting source of molecules for the discovery
27 of antiviral agents [21, 22]. Presently, there are several natural products under efficacy
28 studies for the treatment of Covid-19 [23]. Specifically, diverse plant terpenoids and lignoids
29 demonstrated to be efficacious antivirals against SARS-CoV-1, inhibiting viral replication in
30 vitro, with $IC_{50} \sim 1 \mu M$ [24] and more recently, a series of flavonoids have also been identified
31 as potent inhibitors of SARS-CoV-2 replication in vitro [25].
32
33
34
35
36
37
38
39
40
41
42
43
44
45
46

47 Virtual screening is a reliable procedure for a quick and cost-effective way to discover
48 bioactive compounds from large collections against a specific molecular target [26,27]. A
49 number of *in silico* studies have recently published on the identification of natural products
50 as inhibitors of M^{pro} [28-30]. However, these studies explore a small set of compounds and
51 do not consider protein plasticity, limiting their scope [31]. Moreover, most of these studies
52
53
54
55
56
57
58
59
60

report predictions that still need to be contrasted experimentally [32].

The present work reports the results of a robust *in silico* procedure involving information concerning protein plasticity. Specifically, the study involves a virtual screening of the Selleck database of Natural Compounds containing ~2000 compounds against a set of diverse conformations of the SARS-CoV-2 M^{pro} protease, characterized from a molecular dynamics study. Accordingly, we first report the characterization of the dynamical profile of protease in its *apo* form, using conventional (cMD) as well as gaussian accelerated (GaMD) molecular dynamics simulations, in the form of a set of structure representatives. These structures were subsequently used to carry out ensemble docking. Then, the binding free energy of the most promising candidates was assessed using two different procedures, to finally provide a shortlist of prospective candidates. These compounds were purchased and tested for their ability to inhibit the M^{pro} protease *in vitro*. Accordingly, the present work reports the discovery of five SARS-CoV-2 antivirals, inhibitors of M^{pro} and identified from a database of natural products using a virtual screening procedure.

Methods

1. Computational Studies

1.1 System preparation

The crystallographic structure of SARS-CoV-2 M^{pro} protease (PDB access code 6Y84) was the starting structure for the present study. Although the crystallographic structure is dimeric, since the active site is not affected by the other copy of the protein, we only considered a monomer for present study. Hydrogens were subsequently added to every protein residue at their corresponding protonation state at pH 7.0 and side chains orientations were established using the Protonate3D method [33] embedded in MOE [34]. Next, the protein was placed in a cubic box filled with OPC water molecules [35], setting a minimum distance of 15 Å between the solute and the box walls. Water molecules closer than 1.2 Å to any complex atom were removed. Then, two Na⁺ ions were added to neutralize the system, at the positions of lowest electrostatic potential using the Leap module of

1
2
3 AMBER18 [36]. All calculations were done using the ff19SB force field [37] with a cut-off of
4
5 10 Å for noncovalent interactions, and using the PME method [38] for the treatment of the
6
7 electrostatic interactions.

8 9 1.2 Energy minimization

10
11 Before starting the molecular dynamics calculations, the structure was first relaxed to
12
13 eliminate possible steric clashes in a multistep minimization procedure of 5000 steps each,
14
15 using the steepest descent method. First, only water molecules and ions were allowed to
16
17 relax by keeping fixed all the atoms of the protein applying harmonic positional restrictions
18
19 of 5 kcal/mol·Å⁻². In a second step, only the main atoms of the protein were kept fixed with
20
21 the same harmonic positional restraint as before. Finally, in a third step all the atoms were
22
23 allowed to move.

24 25 1.3 Molecular Dynamics Simulations

26
27 After minimization, the system was heated to 300 K stepwisely at a rate of 30 K every
28
29 20 ps, fixing the main atoms of the protein with a harmonic positional restriction of 0.5
30
31 kcal/mol·Å⁻², using the Langevin thermostat algorithm with a collision frequency of 2 ps⁻¹
32
33 under the NVT ensemble (from now on *heating*). Subsequently, 2 ns simulation was
34
35 performed at constant pressure (NPT ensemble) keeping fixed the main atoms of the protein
36
37 with a harmonic positional restrictions of 0.1 kcal/mol·Å⁻² for density equilibration (from
38
39 now on *density equilibration*). Finally, conventional molecular dynamics (cMD) and gaussian
40
41 accelerated molecular dynamics (GaMD) of 500 ns length were carried out within the NVT
42
43 ensemble in duplicate to increase the explored conformational space of the system [39]. In
44
45 the case of the GaMD simulations, after density equilibration an intermediate step of 20 ns
46
47 was performed to obtain the initial statistical analysis of the dual boost potential. The upper
48
49 limit of the standard deviation of the total potential boost (σ_{0P}) was set to 3 and the upper
50
51 limit of the standard deviation of the dihedral potential boost (σ_{0V}) was set to 5. In these
52
53 simulations, a cutoff of 11 Å was used together with a switch function at 8 Å.

54 55 1.4 Root-Mean Square Deviation (RMSD) and Root-Mean Square Fluctuation (RMSF)

1
2
3 Root-Mean Square Deviation (RMSD) along the simulation time was computed using
4 the cpptraj module [40] from AMBER18 for all the molecular dynamics trajectories to assess
5 the structural stability of the systems along the time. RMSD was computed using the last
6 minimized structure as a reference. However, an iterative procedure was used to select
7 those alpha carbons atoms ($C\alpha$) with smallest fluctuations. Thus, in a first step all $C\alpha$ of the
8 diverse residues were used to reorient the structures. The resulted superposed trajectories
9 were used to calculate the Root-Mean Square Fluctuation (RMSF) for each of the residues of
10 the protein using cpptraj. Residues with a RMSF smaller than a first threshold were selected
11 to be used in the next calculation of the RMSD and so on. Thus, for the first step all the $C\alpha$
12 atoms were used in the superposition but in the next three steps a cut-off of 2.0, 1.0 and 0.5
13 Å, respectively on the RMSF values were used to select the $C\alpha$ to be superposed (Figures S1
14 and S2 of the Supporting Information (SI)). In the last step, a total of 35 amino acids met the
15 desired criteria. This iterative process provides a set of amino acids with small fluctuations
16 along the full MD that can be used to obtain information of the local conformational
17 flexibility for the non-superposed residues.
18
19
20
21
22
23
24
25
26
27
28
29
30

31 *1.5 Cluster Analysis*

32
33
34 In order to select a group of structures representing the greatest structural diversity
35 of the binding site of the M^{pro} protease, similar structures in both the cMD and GaMD
36 simulations were grouped into 15 different clusters using the average linkage algorithm
37 [41], as implemented in the cpptraj module of AMBER18 [36]. For this process, the RMSD of
38 the $C\alpha$ located in the binding site with a larger RMSF was used as distance. A total of 54
39 amino acids were selected (Figure S2 of the SI).
40
41
42
43
44

45 *1.6 Principal Component Analysis*

46
47
48 In order to determine and analyse the extend of the conformational space accessed
49 in the different approaches and understand how different are the representatives selected
50 by our clustering methodology, we used the Principal Component Analysis (PCA). This
51 statistical technique is routinely applied to reduce the number of dimensions needed to
52 describe protein motions from the largest to the smallest spatial scales. First, a covariance
53
54
55
56
57
58
59
60

1
2
3 matrix was constructed including all the structures obtained in the different molecular
4 dynamics and using the atomic coordinates of the C α atoms of the same residues as in the
5 clustering process. Subsequently, the covariance matrix was diagonalized to produce a set
6 of eigenvectors or Principal Components (PC⁽ⁱ⁾, i=1, N), being N the number of selected
7 residues of the protein (in our case 54 residues), as well as their corresponding eigenvalues,
8 $\lambda^{(i)}$. After the eigenvalues are rank ordered, the first components define the “essential” space
9 or motions of the protein [42].
10
11
12
13
14
15

16 17 1. 7. *Virtual screening*

18
19 A multistep virtual screening procedure was performed on each of the seven M^{PRO}
20 representatives selected that is summarized in Figure 1. In step 1, the QVina2 software [43]
21 was used to dock the 1872 molecules of the Natural Products database from Selleck
22 Chemicals [44] in each of the seven target representatives. Molecules from the database had
23 been previously processed to have the right protonation state and their geometries
24 optimized using the MOE software [34]. The docking process was carried out using a
25 rectangular box of dimensions 32.25x31.5x35.25 Å, centred in the middle of the plane
26 defined by the C α of residues Cys¹⁴⁵, Leu²⁷ and His⁴¹. In step 2, we selected those complexes
27 with a scoring function higher than -7.0 kcal/mole in each M^{PRO} representatives. In step 3, the
28 Antechamber and LeaP modules of Amber18 package [36] were used to parametrise the
29 ligands with gaff2 force field [45], solvate the complexes in a box of TIP3P water molecules
30 [46] and add counterions to the complexes, respectively. The ff14SB force field [47] was used
31 to parametrize the protein. Then, each complex was relaxed in a three-step minimization
32 process using 5000 steps in each by means of the steepest descent method. First, only the
33 water molecules and ions were allowed to relax by keeping fixed all the atoms of the protein
34 and ligand applying harmonic positional restrictions of 5 kcal/mol·Å⁻². In a second step only
35 the main atoms of the protein were kept fixed, with a harmonic positional restrain of 5
36 kcal/mol·Å⁻², allowing the ligand to move freely. Finally, in a third step all the atoms were
37 allowed to move. In step 4 of the process, the free energy of binding $\Delta G_{\text{binding}}$ (GB) was
38 computed for all the minimized structures using both the Molecular Mechanics Poisson-
39 Boltzmann Surface Area (MMPBSA) [48] and the Molecular Mechanics Generalized-Born
40
41
42
43
44
45
46
47
48
49
50
51
52
53
54
55
56
57

Surface Area (MMGBSA) [49] procedures. These calculations provide a new scoring to rank order the ligands. Next, we introduced in step 5 a *consensus* criterion to select those complexes that will be studied further using molecular dynamics simulations in step 6. Then, in step 7, a new rank ordered list is obtained after applying the MMGBSA approach to the full length molecular dynamics simulation. Next, an iterative process was done where, at each step, for the best compounds obtained in the previous step their molecular dynamics length was extended and the GB recalculated. In the last step, a final selection of compounds is performed based on their GB for the more extended molecular dynamics and the analysis of the ligand-receptor interactions at the binding site.

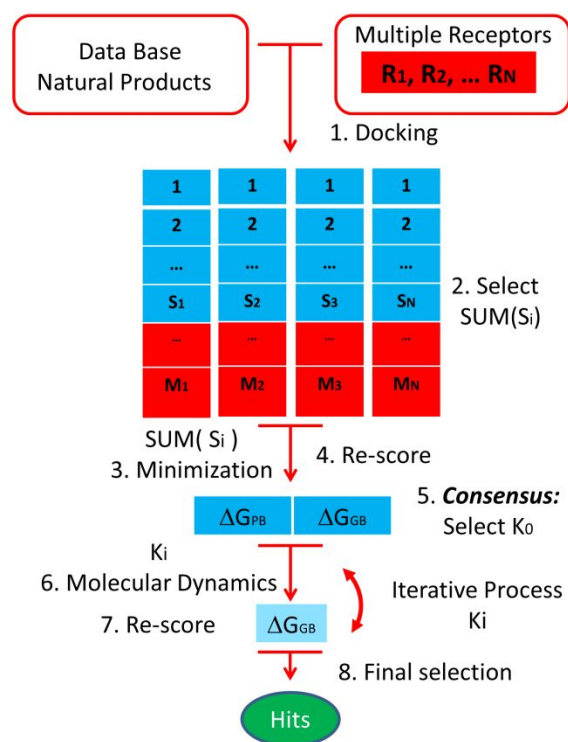


Figure 1. The multi-step Virtual Screening flowchart.

1.8. Binding Free Energy Computation

Binding Free energy was computed using the MMPBSA and the MMGBSA procedures [50], as implemented in the AMBER18 package [36]. In both methods, the free binding energy is computed according to the equation:

$$\Delta G_{binding} = \Delta H^{gas} + \Delta G^{solv} - T\Delta S^{gas}$$

where ΔH^{gas} is the gas-phase interaction energy calculated by summing the internal energy, noncovalent van der Waals ($\Delta H_{vdW}^{\text{gas}}$), and electrostatic ($\Delta H_{elec}^{\text{gas}}$) molecular mechanics energies. On the other hand, ΔG^{solv} is computed as the sum of polar ($\Delta G_{polar}^{\text{solv}}$) and non-polar terms ($\Delta G_{nonpolar}^{\text{solv}}$). The former term is calculated numerically by solving the Poisson-Boltzmann (PB) equation [51] or in its simplified form, the Generalized Born (GB) method [52] for both the MMPBSA and MMGBSA algorithms, respectively. In the present work, we used the Onufriev-Bashford-Case (OBC) generalised Born method (igb=2) [53]. Regarding to $\Delta G_{nonpolar}^{\text{solv}}$, it is calculated using the following equation:

$$\Delta G_{nonpolar}^{\text{solv}} = \gamma \text{SASA} + \beta$$

where SASA is the Solvent-Accessible Surface Area, calculated using the LCPO method [54], and the values for γ and β constants were set to 0.00542 kcal/mol·Å² and 0,92 kcal/mol for MMPBSA [48] and 0.0072 kcal/mol·Å² and 0 kcal/mol for MMGBSA [49]. All the calculations were carried out with the MMPBSA.py program [55].

2. Experimental Procedure

2.1. SARS-CoV-2 M^{pro} expression and purification

M^{pro} was expressed in a pET22b plasmid transformed into BL21 (DE3) Gold *E. coli* strain. Small-scale cultures grown in LB/ampicillin (100 µg/mL) at 37 °C overnight were employed for inoculating 4 L large-scale cultures of LB/ampicillin (100 µg/mL) incubated at 37 °C until reaching OD close to 0.6 at 600 nm. Protein expression was induced with 1 mM isopropyl 1-thio-β-D-galactopyranoside (IPTG) at 18 °C for 5 h. Cells were harvested by centrifugation at 4 °C for 10 min at 10,000 rpm (Beckman Coulter Avanti J-26 XP Centrifuge) and resuspended in lysis buffer (sodium phosphate 50 mM, pH 7, sodium chloride 500 mM). Cells were lysed by sonication (Sonics Vibra-Cell Ultrasonic Liquid Processor) on ice, adding benzonase 20 U/mL (Merck-Millipore) and lysozyme 0.5 mg/mL (Carbosynth). Cell debris was removed by centrifugation at 4 °C for 30 min at 20,000 rpm, and by subsequent filtration (0.45 µm-pore membrane). Affinity chromatography (ÄKTA FPLC System, GE Healthcare Life Sciences) using a cobalt HiTrap TALON column (GE-Healthcare Life

1
2
3 Sciences) allowed fast purification in a single chromatographic step, applying an imidazole
4 10-250 mM gradient. Purity was assessed by SDS-PAGE, and pure protein fractions were
5 pooled and dialyzed to remove imidazole in buffer (sodium phosphate 50 mM, pH 7,
6 sodium chloride 150 mM). Protein concentration was quantitated using an extinction
7 coefficient of $32890 \text{ M}^{-1} \text{ cm}^{-1}$ at 280 nm. Protein identity was assessed by mass spectrometry
8 (LC-ESI-MS/MS).
9
10
11
12
13
14
15

16 2.2. SARS-CoV-2 M^{pro} proteolytic activity assay

17

18 A continuous assay based on Förster resonance energy transfer (FRET) to measure *in*
19 *vitro* the catalytic activity of M^{pro} was implemented by using the substrate
20 (DabcyI)KTSAVLQSGFRKME(Edans)-NH₂ (Biosyntan GmbH). The enzymatic reaction
21 was initiated by adding substrate at 20 μM (final concentration) to the enzyme at 0.2 μM
22 (final concentration) in a final volume of 100 μL . The reaction buffer was sodium phosphate
23 50 mM, pH 7, NaCl 150 mM. For compounds dissolved in pure DMSO as stock solution, a
24 constant DMSO percentage (2.5%) was kept in all assays. Fluorescence emission was
25 measured in a FluoDia T70 microplate reader (Photon Technology International) for 20 min
26 (excitation wavelength, 380 nm; emission wavelength, 500 nm). The initial slope of the time
27 evolution curve of the fluorescence emission signal provided a direct quantification of the
28 enzymatic activity. The Michaelis-Menten constant, K_m , and the catalytic rate constant or
29 turnover number, k_{cat} , were previously estimated ($K_m = 11 \mu\text{M}$ and $k_{\text{cat}} = 0.040 \text{ s}^{-1}$).
30
31
32
33
34
35
36
37
38
39
40
41

42 2.3. SARS-CoV-2 M^{pro} inhibition assay

43

44 The *in vitro* inhibition potency of the compounds against M^{pro} was assessed through
45 the estimation of the inhibition constant, K_i , and the half-maximal inhibitory concentration,
46 IC_{50} , from experimental inhibition curves. Inhibition curves were obtained by measuring the
47 enzyme activity (at fixed 0.2 μM enzyme concentration and fixed 20 μM substrate
48 concentration) as a function of compound concentration (serial 2-fold dilution from 125 μM
49 to 0 μM), maintaining the percentage of DMSO constant (2.5%) for compounds dissolved in
50 DMSO. The enzymatic activity was quantitated as the initial slope of the substrate
51
52
53
54
55
56
57
58
59
60

fluorescence emission time evolution curve, and was plotted as a function of compound concentration. The ratio between the activity (slope) in the presence and absence of compound provides the residual percentage of activity at a given compound concentration. Non-linear regression analysis employing a simple inhibition model (considering inhibitor depletion due to enzyme binding) allowed us to estimate the apparent inhibition constant, K_i^{app} , for each compound, according to Equation 1:

$$\begin{aligned}
 [EI] &= \frac{1}{2} \left([I]_T + [E]_T + K_i^{\text{app}} - \sqrt{([I]_T + [E]_T + K_i^{\text{app}})^2 - 4[E]_T[I]_T} \right) \\
 [I] = [I]_T - [EI] &= \frac{1}{2} \left([I]_T - [E]_T - K_i^{\text{app}} + \sqrt{([I]_T + [E]_T + K_i^{\text{app}})^2 - 4[E]_T[I]_T} \right) \quad (1) \\
 \frac{v([I])}{v([I]=0)} &= 1 - \frac{[EI]}{[E]_T} = \frac{1}{1 + \frac{[I]}{K_i^{\text{app}}}}
 \end{aligned}$$

where $[EI]$ is the concentration of the enzyme-inhibitor complex, $[E]_T$ and $[I]_T$ are the total concentrations of enzyme and inhibitor, K_i^{app} is the apparent inhibition constant for the inhibitor, $[I]$ is the concentration of free inhibitor, and v is the initial slope of the enzymatic activity trace at a given (free) inhibitor concentration $[I]$ (or total inhibitor concentration $[I]_T$). No approximation for the free inhibitor concentration (e.g., assuming to be equal to the total inhibitor concentration) was made, thus having general validity for any total enzyme and inhibitor concentration and any value of the inhibition constant. In addition, if the inhibitor acts through a purely competitive mechanism, the previous equation can be substituted by Equation 2:

$$\frac{v([I])}{v([I]=0)} = \frac{1}{1 + \frac{[I]}{K_i^{\text{app}}}} = \frac{1}{1 + \frac{[I]}{K_i \left(1 + \frac{[S]}{K_m} \right)}} \quad (2)$$

where K_i is the intrinsic (i.e., substrate concentration-independent) inhibition constant, K_m the Michaelis-Menten constant for the enzyme-substrate interaction, and $[S]$ the substrate concentration. By approximating the free compound concentration by the total compound concentration and neglecting ligand depletion, the K_i^{app} in equation 2 is equivalent to the IC_{50} . It should be noted that, as the IC_{50} is an assay-dependent inhibition potency index

(among other parameters, it depends on the enzyme and substrate concentrations, as well as on the K_m), the intrinsic inhibition constant is a better inhibition potency index.

Purity of the compounds tested

The 11 compounds tested in the present study were purchased from Selleck Chemicals (Houston, TX, USA). All compounds are >95% pure by HPLC. HPLC traces for representative compounds is included in the SI.

Results and Discussion

Selection of Structures Representing M^{pro} Plasticity

A clustering process was performed for both conventional (cMD) and gaussian accelerated (GaMD) molecular dynamics calculations separately, as explained in the methods section to identify representative structures of the most populated clusters. We previously had performed an iterative process to select the set of atoms to be involved in the superposition process, bearing in mind to cover the maximum conformational diversity of the binding site in the selected representatives (Figure S1 of the SI). Thus, we iteratively selected the atoms involved in the superposition process according to their RMSF (Figure S2 of the SI). After the last step, 35 amino acids located in the binding site with small fluctuations along the MD trajectory were selected to superimpose the structures (Figure S3 of the SI). Once the superposition was performed using the corresponding $C\alpha$, the RMSD of a total of 54 amino acids located in the binding site with large RMSF values was used as distance for the clustering process (Figures S2 and S3 of the SI). Three and four representatives were selected for both the cMD and GaMD, respectively, representing clusters with more than a 10% population. Despite assessment of the conformational diversity of our selected structures can be done by visual inspection (Figure S4 of the SI), we used Principal Component Analysis (PCA) to get a clearer picture. For this purpose, we analysed the RMSF of the amino acids located on the binding site. Those amino acids with lower RMSF were used for superimposition of the structures, whereas those with larger RMSF were used for the computation of the covariance matrix (Figure S3 of the SI). As shown in Figure 2, the conformational space covered by cMD and GaMD is markedly different, a fact that is further stressed after using two MD runs for each approach. Thus,

the representatives selected will describe a broad range of situations where the ligands can bind.

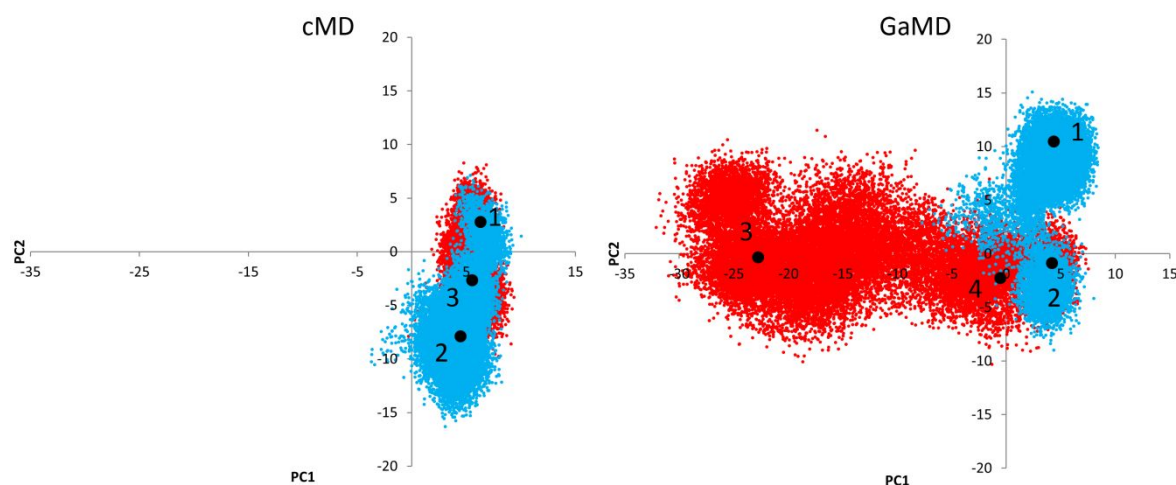


Figure 2. Representation of the first two Principal Components (PC) sampled by cMD and GaMD approaches. Blue and red indicate the two different MD. The big black points are the positions of the selected representatives for the clusters with more than 10% of the total population; three for the cMD and four for the GaMD.

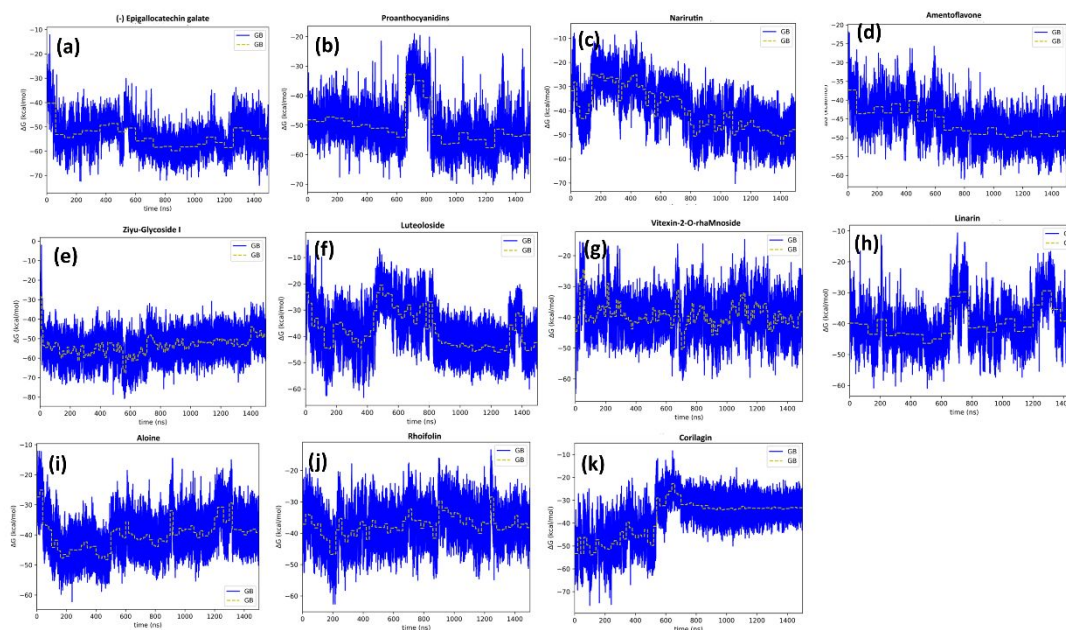
Virtual Screening Targeting the SARS-Cov-2 M^{pro} Protease.

The QVina2 software [43] was used to perform ensemble docking of the diverse molecules from the Natural Product database onto the seven M^{pro} structural representatives and compute their corresponding scoring function values. For each structure representative, those ligand-M^{pro} complexes with a scoring function lower or equal to an established threshold were rank ordered and conserved for further analysis. A threshold of -7.0 kcal/mol was established after analysis of the results produced for the most populated cluster representative identified from the cMD. Specifically, the plot of the cumulative number of complexes obtained versus their scoring function value (see in Figure S5 of the SI), shows that there are already around 500 complexes values with -7.0 kcal/mol or lower, that represents a number large enough to include chemical diversity and permits to keep the computational cost at a reasonable size. Complexes selected may include more than one pose per compound, and actually, the same compound may appear in the rank ordered list of different representatives. Application of the threshold to the different M^{pro} structures yields different number of complexes for each structure. Specifically, 513, 878 and 637 for

1
2
3 the three cMD representatives and 558, 1840, 949 and 293 for the four GaMD representatives.
4

5 Ligand-receptor complexes selected from the docking process were subsequently
6 subjected to a minimization process in explicit water, allowing complete conformational
7 freedom for both the ligand and the protease. The binding energy of the minimized
8 structures was subsequently computed using the end-point methodologies MMPBSA [48]
9 ($\Delta G_{\text{binding}}(\text{PB})$) and MMGBSA [49] ($\Delta G_{\text{binding}}(\text{GB})$). Thus, at the end of this process we
10 produced two rank ordered lists for each M^{Pro} representative structure, giving a total of 14
11 lists. Selection of the set of prospective binders was performed following a *consensus*
12 approach. The procedure is based on the assumption that the larger the number of target
13 conformations a ligand binds, the higher its chances of being a hit. Accordingly, we did not
14 select directly compounds with the lowest binding energy, but those ligands that exhibit
15 binding to diverse conformations of the target within the threshold. Using this criterion, we
16 selected 47 compounds that exhibit binding to all 7 structural representatives of the target,
17 together with additional 21 compounds that exhibit binding to six out of the seven structural
18 representatives, producing a total of 68 compounds. For each compound, we selected the
19 complex structure with the lowest binding energy for further studies.
20
21
22
23
24
25
26
27
28
29
30
31
32
33

34 The 68 selected complex structures were prepared for the production step as described
35 in section 1.3. Thus, a *heating* from 0 K to 300 K and a *density equilibration* for each one was
36 carried out before a 100 ns of production molecular dynamics simulation. After completion,
37 the $\Delta G_{\text{binding}}(\text{GB})$ time evolution of every compound was computed using the MMGBSA
38 approach. Analysis of these plots shows that 38 out of the 68 ligand-protease complexes
39 either exhibit a smooth fluctuating behaviour during the last 20 ns. In order to reduce the
40 final number of candidates, these 38 complexes were selected to extend their MD
41 simulations up to 200 ns. After analysis of the $\Delta G_{\text{binding}}(\text{GB})$ behaviour and using the same
42 criterion, 21 ligand-protease complexes were selected for another round of MD simulations,
43 extending them up to 500 ns. In a final step, using the same criterion, only 11 complexes
44 were selected for extending their MD simulations up to 1.5 μs to check the smooth behaviour
45 of the free energy of binding previously observed.
46
47
48
49
50
51
52
53
54
55
56
57
58
59
60



Figures 3a-3k. Time evolution of the binding free energy of the 11 compounds selected from the virtual screening process.

Compounds were selected after inspection of the time evolution of the binding free energy during the MD simulation. A smooth behaviour with small fluctuations around the mean are considered as indication of good candidates, although some of the compounds show important fluctuations that are corrected at the end of the respective simulations. The time evolution of $\Delta G_{\text{binding}}$ (GB) for the 11 selected complexes using the MMGBSA approach is shown in Figures 3a-3k.

After analysis of the time evolution plots, 11 compounds were selected as prospective candidates resulting from the virtual screening process, including (-) epigallocatechin gallate (**1**) (This refers to (2R,3R)-5,7-Dihydroxy-2-(3,4,5-trihydroxyphenyl)-3,4-dihydro-2H-1-benzopyran-3-yl 3,4,5-trihydroxybenzoate, the major polyphenolic catechin found in green tea), proanthocyanidins (**2**), narirutin (**3**), amentoflavone (**4**), ziyu-glycoside I (**5**), luteoloside (**6**), vitexin-2-O-rhamnoside (**7**), linarin (**8**), aloin (**9**), rhoifolin (**10**) and corilagin (**11**) (Figure 4).

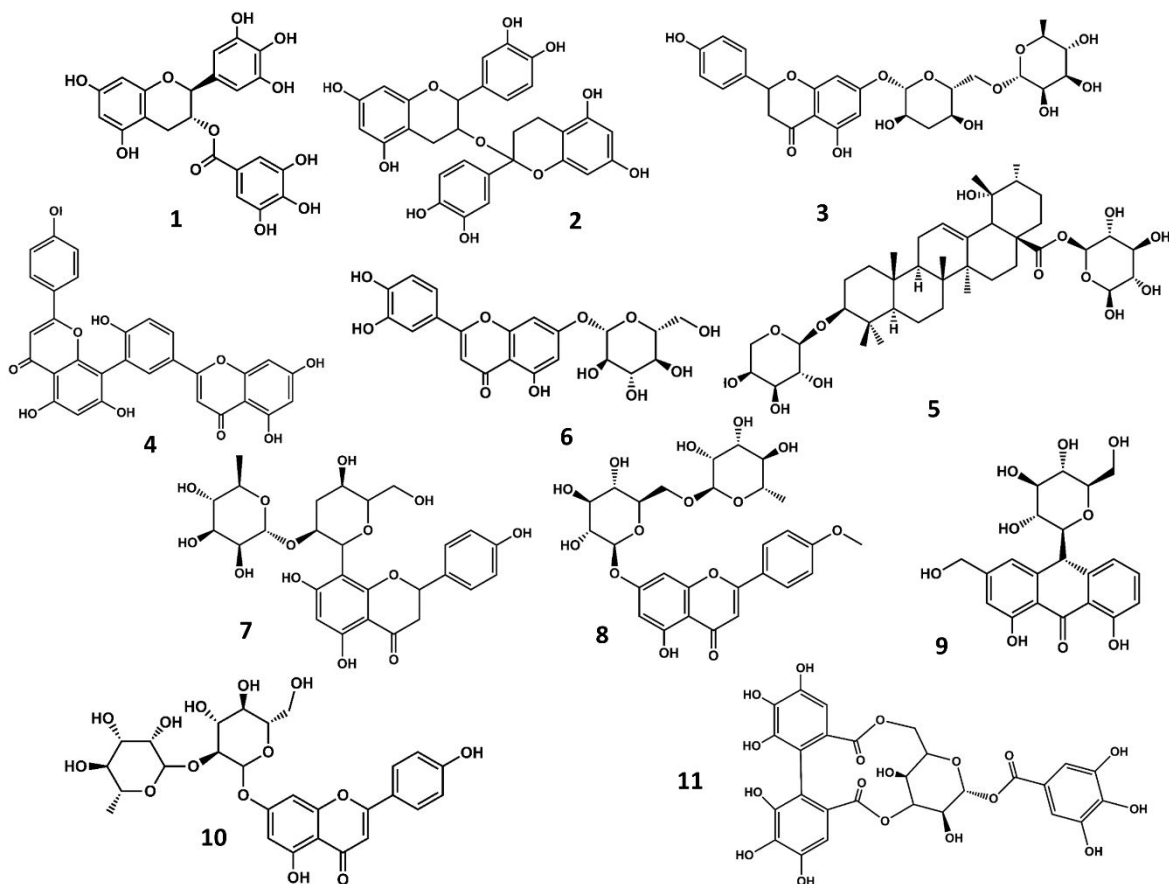


Figure 4. Chemical structures of the natural compounds identified as prospective hits targeting the M^{pro} protease from the virtual screening process. (-) epigallocatechin gallate (1), proanthocyanidins (2), narirutin (3), amentoflavone (4), ziyu-glycoside I (5), luteoloside (6), vitexin-2-O-rhamnoside (7), linarin (8), aloin (9), rhoifolin (10) and corilagin (11)

In vitro M^{pro} inhibitory activity of candidate compounds

The 11 prospective candidates identified from the virtual screening process were purchased and tested in an *in vitro* assay. Specifically, the inhibitory potential of the compounds against recombinant SARS-CoV-2 M^{pro} was tested by a Förster resonance energy transfer (FRET) assay, as described in the methods section. Five compounds showed specific inhibitory activity, with substrate concentration-independent inhibition constants (K_i) ranging from 7.8 μ M for (-) epigallocatechin gallate to 82 μ M for aloin. The remaining seven compounds did not yield detectable inhibitory activities at concentrations below 125

1
2
3 μM . Table 1 lists their measured activity together with their binding energy computed as
4 described in the methods section. Inhibition curves are shown in Figure S6 of the SI.
5
6
7

8 **Table 1.** *in vitro* inhibition values exhibited by the diverse compounds purchased rank ordered by their
9 computed binding energies. Compounds with no detectable inhibitory activity at concentrations below 125 μM
10 are marked with an asterisk.
11
12

Compound	$K_i(\mu\text{M})$	$\text{IC}_{50}(\mu\text{M})$	$\Delta G_{\text{binding}}(\text{GB})$ (kcal/mol)
(-) Epigallocatechin gallate	7.8	22	-54.6
Proanthocyanidins	*	*	-52.9
Narirutin	*	*	-48.9
Amentoflavone	10	28	-48.5
Ziyu-glycoside I	*	*	-48.1
Luteoloside	*	*	-43.6
Vitexin-2-O-rhamnoside	23	65	-40.9
Linarin	*	*	-39.6
Aloin	34	96	-38.9
Rhoifolin	82	230	-36.9
Corilagin	*	*	-33.4

13
14
15
16
17
18
19
20
21
22
23
24
25
26
27
28
29
30
31
32 Inspection of Table 1 shows that there is a correlation for the active compounds
33 between the computed binding energy to the M^{pro} protease and their inhibitory capacity *in*
34 *vitro*. However, despite having reasonable binding affinities, several of the listed
35 compounds do not exhibit inhibitory activity. Actually, the procedure followed to identify
36 active compounds yields a 45% success rate, as previously found in similar studies [56, 57].
37 This can be attributed to diverse factors related to the physicochemical properties of the
38 compounds like solubility or lipophilicity profile among others that may prevent reaching
39 the target in the conditions of the experiment. Among the compounds reported in the
40 present study, (-) epigallocatechin gallate [58-60] and rhoifolin [61] have already been
41 reported as M^{pro} protease inhibitors from screening studies. Moreover, vitexin has also been
42 proposed as a prospective M^{pro} inhibitor from modelling studies [62]. The rest of the active
43 compounds are disclosed in the present work for the first time.
44
45
46
47
48
49
50
51
52
53

54
55 As previously shown, the procedure used in the present work to select prospective
56
57

1
2
3 candidates is based on the behavior of the time evolution of the ligand-M^{PRO} complex binding
4 free energy. Fluctuations are associated to the movement the ligands experience inside the
5 binding pocket. Specifically, when time evolution of the binding free energy is smooth it
6 fluctuates ~20 kcal/mol around an average value and it is stable with time. These
7 fluctuations can be associated with ligand rattling inside the binding pocket but bound in a
8 specific pose. Ligands of this category are considered for experimental evaluation. Larger
9 fluctuations may be associated with a lack of steric complementarity between the ligand and
10 the protein binding pocket, so that ligands have lower chances to become hits. In contrast,
11 abrupt changes are associated with the accommodation of the ligand inside the binding
12 pocket. When the subsequent behavior is stable, ligands are considered for experimental
13 evaluation. In contrast, if fluctuations persist, ligands are discarded as candidates. Finally,
14 behaviors where the binding free energy does not get a stable average behavior have lower
15 chances to become hits. In summary, this procedure relies on the ligand bound residence
16 time as indicator of the chances for a ligand to be a hit and represents a more a robust
17 discrimination procedure than using only the predicted binding free energy. Thus, (-
18)epigallocatechin gallate, the most active compound identified in this study, exhibits a
19 smooth time evolution (Figure 3a) with fluctuations around 20 kcal/mol. Similarly, plots of
20 the other active compounds including amentoflavone (Figure 3d), vitexin-2-rhamnoside
21 (Figure 3g), aloin (Figure 3i) and rhoifolin (Figure 3j) show stable behaviors. The only
22 exception to this criterion is represented by ziyu-glucoside I that despite exhibiting a stable
23 time evolution (Figure 3g) the compound turns out to be non-active in the experimental test.

24
25
26
27
28
29
30
31
32
33
34
35
36
37
38
39
40
41
42
43 Regarding the non-active compounds, inspection of the time evolution of the free
44 energy of binding can provide hints of their lack of inhibitory capacity. Specifically,
45 inspection of the proanthocyanidins plot (Figure 3b) shows a large fluctuation around 700
46 ns as a sign of instability. Despite the average binding free energy comes back to previous
47 values the system exhibits fluctuations larger than 20 kcal/mole. In this case, the compound
48 turns out to be non-active despite exhibiting a good binding free energy. The plot of linarin
49 (Figure 3h) shows several fluctuations that suggest positional changes of the ligand inside
50 the binding pocket that can explain its lack of activity. The behavior of corilagin (Figure 3k)

1
2
3 suggests that the ligand, despite showing a stable behavior after 600 ns is subjected to
4 conformational changes that produce a loss of stability from the starting position. On the
5 other hand, narirutin and luteoloside exhibit a time evolution binding free energy plots
6 (Figures 3c and 3f, respectively) that are not converged after 1.5 μ s simulation time.
7
8
9

10
11 The prospective bound conformation of the five ligands found to be active onto the
12 active site of M^{pro} is shown in Figures 5-9. Specifically, these structures correspond to the
13 last snapshot of the corresponding 1.5 μ s molecular dynamics trajectory. Inspection of
14 Figures 5-9 suggests that ligands occupy common spots of the binding site including the S1'
15 and S1 and/or S2 subsites [20], although some of the residues involved in ligand-enzyme
16 interactions can be different for the diverse ligands. Thus, all the ligands occupy the S1'
17 subsite, location of the catalytic dyad Cys¹⁴⁵ and His⁴¹, establishing hydrogen bond
18 interactions with the former and quadrupole-quadrupole interactions with the latter.
19 Furthermore, other residues like Glu¹⁶⁶ (located in the S1 subsite) or Gln¹⁴² together with
20 Asp¹⁸⁷ (located in the S2 subsite) establish hydrogen bonds with some of the ligands, as
21 summarized in Table S1 of the SI. Interestingly, the ligand amentoflavone due to its size also
22 occupies the S4 subsite of the binding site. All these residues have already been reported as
23 important for designing novel M^{pro} inhibitors [20, 63].
24
25
26
27
28
29
30
31
32
33
34
35

36 The most active compound, (-) epigallocatechin gallate (Figure 5) occupies subsites
37 S1', S1 and S2 establishing multiple interactions with different residues of the enzyme.
38 Specifically, the ligand exhibits hydrogen bonds with Asp⁴⁸, Cys¹⁴⁵, His¹⁶⁴, Glu¹⁶⁶ and Asp¹⁸⁷
39 together with a quadrupole-quadrupole interaction with His⁴¹, exhibiting complementary
40 stereochemical features with the protease binding site.
41
42
43
44
45
46
47
48
49
50
51
52
53
54
55
56
57
58
59
60

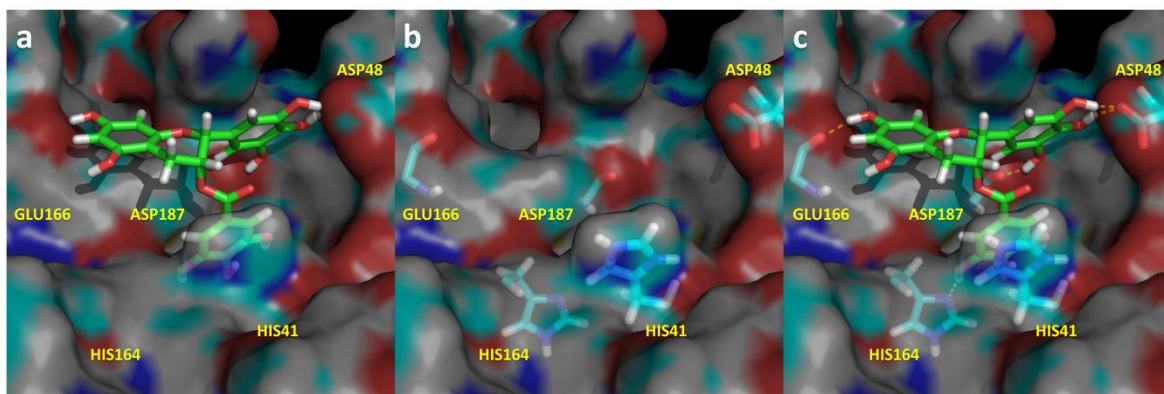


Figure 5. Spatial representation of the complex M^{Pro}-(-) epigallocatechin gallate in its last snapshot of the 1.5 μ s molecular dynamics. a) Ligand bound to the binding pocket; b) Spatial distribution of the most important residues that interact with the ligand; c) Ligand-protease hydrogen bonds in yellow.

Amentoflavone (Figure 6) occupies subsites S1', S1, S2 and S4 establishing multiple hydrogens bonds with different residues of the enzyme including Cys⁴⁴, Asn¹⁴², Cys¹⁶⁵ and Glu¹⁶⁶ together with a quadrupole-quadrupole interaction with His⁴¹.

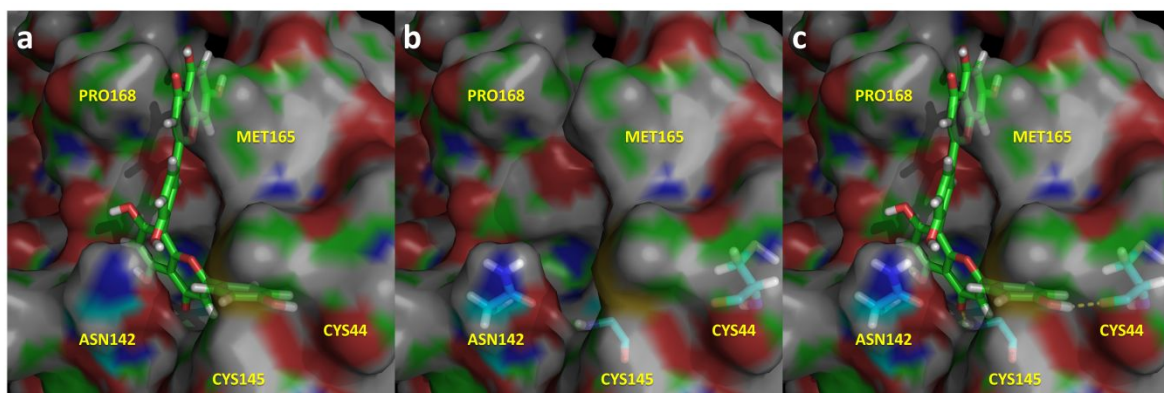


Figure 6. Spatial representation of the complex M^{Pro}-Amentoflavone in its last snapshot of the 1.5 μ s molecular dynamics. a) Ligand bound to the binding pocket; b) Spatial distribution of the most important residues that interact with the ligand; c) Ligand-protease hydrogen bonds in yellow.

Vitexin-2-O-rhaMnoside (Figure 7) occupies subsites S1' and S1 establishing multiple hydrogens bonds with different residues of the enzyme including Ser⁴⁶, Ser¹⁴⁴, Cys¹⁴⁵, His¹⁶⁴, Glu¹⁶⁶ and Asp¹⁸⁷ together with a quadrupole-quadrupole interaction with His⁴¹.

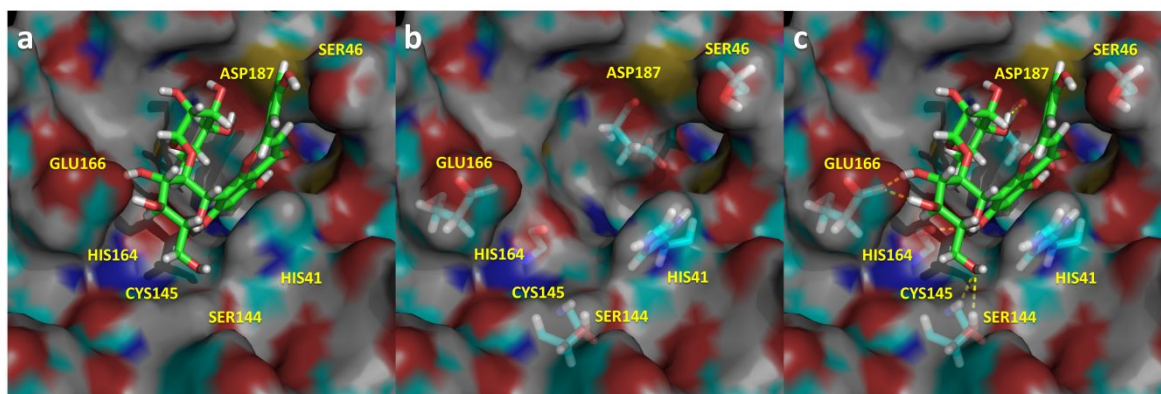


Figure 7. Spatial representation of the complex M^{Pro}-Vitexin-2-O-rhaMnoside in its last snapshot of the 1.5 μ s molecular dynamics. a) Ligand bound to the binding pocket; b) Spatial distribution of the most important residues that interact with the ligand; c) Ligand-protease hydrogen bonds in yellow.

Aloin (Figure 8) also occupies subites S1' and S1, establishing multiple hydrogens bonds with different residues of the enzyme including Ser⁴⁶, Met⁴⁹, Ser¹⁴⁴, Cys¹⁴⁵, Met¹⁶⁵, Asp¹⁸⁷ and Gln¹⁸⁹ together with a quadrupole-quadrupole interaction with His⁴¹.

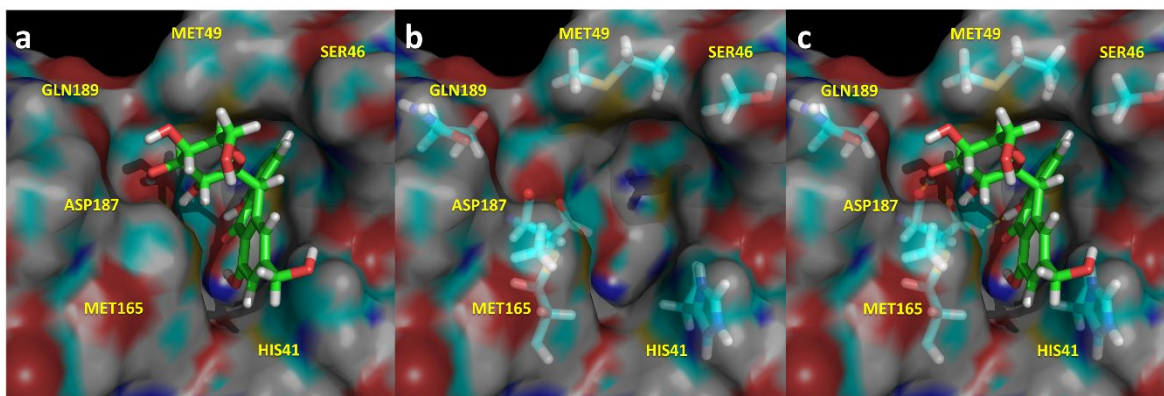


Figure 8. Spatial representation of the complex M^{Pro}-Aloin in its last snapshot of the 1.5 μ s molecular dynamics. a) Ligand bound to the binding pocket; b) Spatial distribution of the most important residues that interact with the ligand; c) Ligand -protease hydrogen bonds in yellow.

Rhiofolin (Figure 9) occupies subsites S1' and S2, establishing multiple hydrogens bonds with different residues of the enzyme including Met⁴⁹, Asn¹⁴², Gly¹⁴³, Cys¹⁴⁵, Glu¹⁶⁶, Gln¹⁸⁹ and Lys²³⁶ together with a quadrupole-quadrupole interaction with His⁴¹.

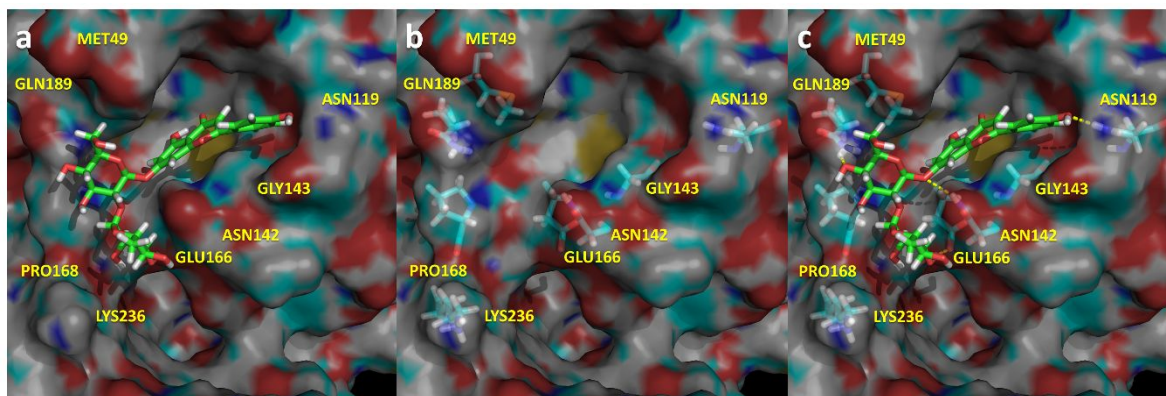


Figure 9. Spatial representation of the complex M^{Pro}-Rhiofolin in its last snapshot of the 1.5 μ s molecular dynamics. a) Ligand bound to the binding pocket. b) Spatial distribution of the most important residues that interact with the ligand. c) Ligand -protease hydrogen bonds in yellow.

This qualitative description of ligand-enzyme interactions can be further reinforced through the analysis of the individual residue contributions to the binding free energy shown in Figures 10a-10e. Binding interaction for each residue-residue pair includes three terms: van der Waals contribution, electrostatic contribution and solvation contribution. The polar contribution of ΔG_{solv} was computed as in the case of the ΔG_{bind} using the generalized Born model based on the parameters developed by Onufriev et al. [53]. All energy components were calculated using 25000 snapshots corresponding to the last 100 ns of the full-length molecular dynamics run.

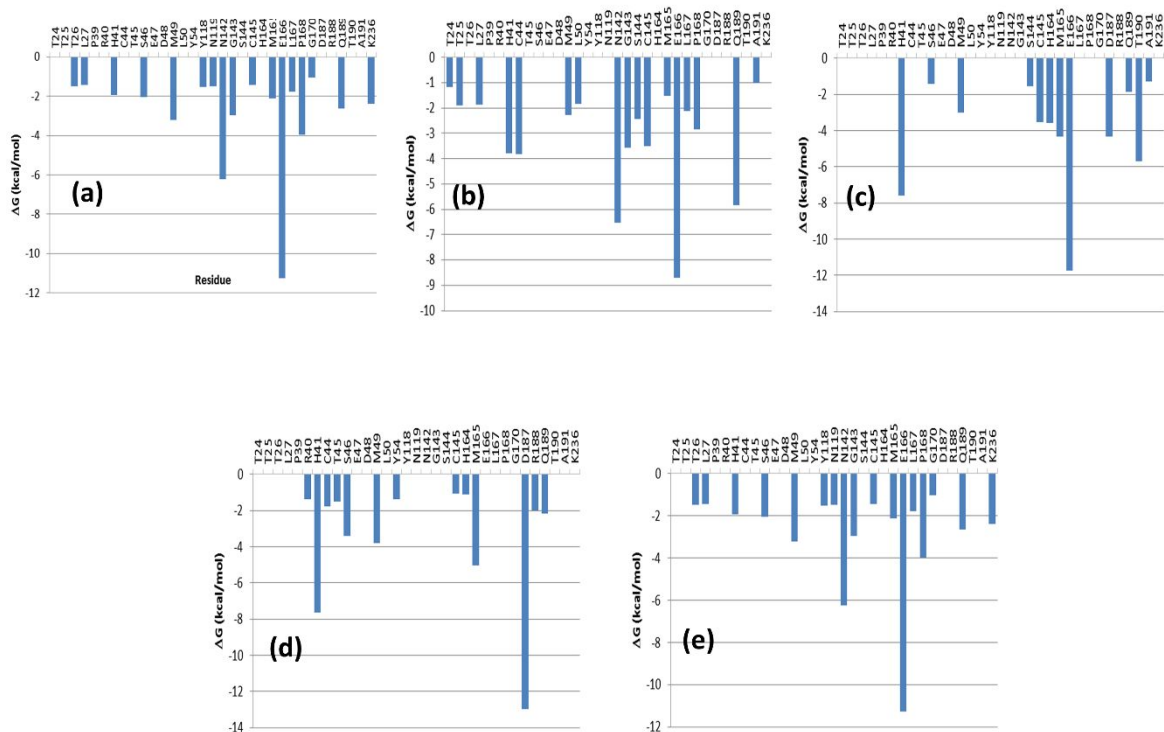


Figure 10. Residue decomposition of the binding free energy interaction for the diverse ligand-MP^{Pro} protease complexes found active. a) (-) epigallocatechin gallate; b) amentoflavone; c) vitexin-2-O-rhaMnoside; d) aloin; e) rhoifolin.

Analysis of Figures 10a-10e shows that not all the compounds exhibit the same pattern of interactions, although there are specific residues relevant for binding that are common to all the compounds. Thus, these plots corroborate the involvement of dyad residues Cys¹⁴⁵ and His⁴¹ in all the complexes. Moreover, the relevance of residue Glu¹⁶⁶ and in some cases Asn¹⁴² or Asp¹⁸⁷ as ligand anchoring points is also underlined, as previously described. Actually, Glu¹⁶⁶ is an important contributor to the binding energy of compounds like (-) epigallocatechin gallate, amentoflavone, vitexin-2-O-rhaMnoside and rhoifolin, whereas the Asn¹⁴² is important for (-) epigallocatechin gallate, amentoflavone and rhoifolin, whereas Asp¹⁸⁷ is an important contributor for vitexin-2-O-rhaMnoside and aloin. Interestingly, there

1
2
3 are residues like Met⁴⁹ or Pro¹⁶⁸ that make a remarkable contribution to the binding energy
4 of the ligands through van der Waals interactions.
5
6

7
8 Inspection of Table S1 of the SI also suggests the capacity of these ligands to form
9 hydrogen bonds as a consequence of the high number of alcohol moieties they exhibit.
10 Moreover, these molecules belong to chemical class of polyphenols, considered to have
11 antiviral, antibacterial, antioxidant, and anti-inflammatory activities. Specifically, diverse
12 studies have investigated their potential antiviral efficiency against SARS-CoV-2 with
13 varied results. Specifically, (-) epigallocatechin gallate [58-60] and rhoifolin [61] were
14 previously identified as a M^{Pro} inhibitors, although other polyphenols may act as ligands of
15 different enzymes [64].
16
17
18
19
20
21

22 **Conclusions**

23
24

25 The need for availability of compounds that can be used as therapeutical agents for
26 the treatment of Covid-19 prompted to screen for approved drugs and natural products.
27 Virtual screening is a cost-effective technique to screen for large libraries of compounds. The
28 purpose of this work was to carry out virtual screening of the Selleck library of Natural
29 Compounds using the M^{Pro} protease of SARS-CoV-2 as target aimed at identifying
30 prospective antivirals. For this purpose, we carried out an ensemble docking of ca. 2000
31 compounds using 7 different structures characterizing the plasticity of the M^{Pro} binding
32 pocket. Compounds showing binding to 6 or 7 of the diverse M^{Pro} structures and with a
33 scoring function above a threshold were selected for further analysis. After this process, we
34 analyzed about 68 compounds that were screened according to the behavior of the binding
35 free energy along a molecular dynamics process. Finally, 11 compounds were purchased
36 and tested in vitro, for their capability to inhibit the M^{Pro} protease. The results show that 5
37 out the 11 are active that gives a 45% success rate.
38
39
40
41
42
43
44
45
46
47
48
49

50 The resulting active 5 compounds were analyzed to identify residues responsible for
51 their activity. Two analyses were done. On the one hand, one more qualitative from
52 inspection of the prospective bound conformation of the ligands inside the M^{Pro} binding
53 pocket and another, more quantitative where the binding free energy is decomposed in
54
55
56
57

1
2
3 residue contributions. The results show that dyad residues Cys¹⁴⁵ and His⁴¹ are involved in
4 all the complexes and that Glu¹⁶⁶ and Asn¹⁸⁷ play an important role in the affinity of this
5 group of inhibitors. Finally, other residues including Met⁴⁹, Asn¹⁴² or Pro¹⁶⁸, despite not
6 being in direct contact with the ligands they interact with other residues playing a relevant
7 role in defining the M^{Pro} binding pocket.
8
9
10
11

12 13 **Data and Software Availability**

14
15
16 Coordinates of the 7 structures of M^{Pro} protease identified in the cluster analysis, as
17 well as of the 11 ligand-M^{Pro} complexes studied in this work are provided in pdb format
18 upon request to the authors.
19
20
21

22 **Supporting Information Available**

23
24
25 Diverse information regarding the computational procedure followed, as well as
26 details on the results produced in the *in vitro* studies are available as supplementary
27 material.
28
29
30

31 **Acknowledgments**

32
33
34 This study was supported by The Agència de Gestió d' Ajuts Universitaris i de Recerca
35 (AGAUR)-Generalitat de Catalunya (2017SGR1033) and Spanish Structures and Excellence
36 María de Maeztu program, grant number MDM-2017-0767. Fundación hna (to A.V.C. and
37 O.A.). Miguel Servet Program from Instituto de Salud Carlos III (CPII13/00017 to O.A.);
38 Fondo de Investigaciones Sanitarias from Instituto de Salud Carlos III, and European Union
39 (ERDF/ESF, 'Investing in your future') (PI18/00349 to O.A. and a FIS Research Contract to
40 L.C.L.). Spanish Ministry of Economy and Competitiveness (BFU2016-78232-P to A.V.C.).
41 Spanish Ministry of Science, Innovation and Universities (FPI Predoctoral Research
42 Contract BES-2017-080739 to D.O.A.). Diputación General de Aragón (Predoctoral Research
43 Contract 2019 to A.J.A., 'Protein Targets and Bioactive Compounds Group' E45_20R to
44 A.V.C., 'Digestive Pathology Group' B25_20R to O.A.). Centro de Investigación Biomédica
45 en Red en Enfermedades Hepáticas y Digestivas (CIBERehd to T.M.T, O.A. and A.V.C.).
46
47
48
49
50
51
52
53
54
55
56
57
58
59
60

1
2
3 Consejo Superior de Investigaciones Científicas (COV-006 and COV-201 to T.M.T.). Agència
4 de Gestió d'Ajuts Universitaris i de Recerca (2020PANDE00048 to J.R.M and T.M.T.). Plan
5 Nacional de I+D (PID-107139RB-C21 to T.M.T.). JJP likes to acknowledge the Government
6 of Catalonia (2017 SGR 163) and the Instituto de Salud Carlos III (COV20/00052) for financial
7 support.
8
9
10
11
12
13
14
15
16
17
18
19
20
21
22
23
24
25
26
27
28
29
30
31
32
33
34
35
36
37
38
39
40
41
42
43
44
45
46
47
48
49
50
51
52
53
54
55
56
57
58
59
60

References

1. Susan Payne. Viruses: From Understanding to Investigation. Chapter 17 - Family Coronaviridae. Academic Press, pp 149-158. New York, **2017**,
2. de Wit, E., van Doremalen, N., Falzarano, D., Munster, V. J. SARS and MERS: recent insights into emerging coronaviruses. *Nat. Rev. Microbiol.* **2016**, *14*, 523-534
3. World Health Organization. General's Opening Remarks at the Media Briefing on COVID-19-18 March 2020; World Health Organization: Geneva, Switzerland, **2020**.
4. COVID-19 Dashboard by the Center for Systems Science and Engineering (CSSE) at Johns Hopkins University (JHU). Available on-line at: <https://coronavirus.jhu.edu/map.html>. (accessed on June 20th **2021**)
5. Riva, L., Yuan, S., Yin, X. et al. Discovery of SARS-CoV-2 antiviral drugs through large-scale compound repurposing. *Nature.* **2020**, *586*, 113–119.
6. Bugin, K., Woodcock, J. Trends in COVID-19 therapeutic clinical trials. *Nat. Rev. Drug Discov.* **2021**, *20*, 254-255.
7. Li, G., De Clercq, E. Therapeutic options for the 2019 novel coronavirus (2019-nCoV). *Nat. Rev. Drug Discov.* **2020**, *19*, 149-150.
8. Scavone, C., Brusco, S., Bertini, M., Sportiello, L., Rafaniello, C., Zoccoli, A., Berrino, L., Racagni, G., Rossi, F., Capuano, A. Current pharmacological treatments for COVID-19: What's next? *Br. J. Pharmacol.* **2020**, *177*, 4813–4824.
9. McKee, D. L., Sternberg, A., Stange, U., Laufer, S., Naujokat, C. Candidate drugs against SARS-CoV-2 and COVID-19. *Pharmacol. Res.* **2020**, *157*, 104859
10. Beigel, J.H., Tomashek, K.M., Dodd, L.E., Mehta, A.K., Zingman, B.S., Kalil, A.C., Hohmann, E., Chu, H.Y., Luetkemeyer, A., Kline, S., Lopez de Castilla, D., Finberg, R.W., Dierberg, K., Tapson, V., Hsieh, L., Patterson, T.F., Paredes, R., Sweeney, D.A., Short, W.R., Touloumi, G., Lye, D.C., Ohmagari, N., Oh, M., Ruiz-Palacios, G.M., Benfield, T.,

1
2
3 Fätkenheuer, G., Kortepeter, M.G., Atmar, R.L., Creech, C.B., Lundgren, J., Babiker, A.G.,
4 Pett, S., Neaton, J.D., Burgess, T.H., Bonnett, T., Green, M., Makowski, M., Osinusi, A.,
5 Nayak, S., Lane, H.C. Remdesivir for the Treatment of Covid-19- Preliminary Report. *N.*
6 *Engl. J. Med.* **2020**, *383*, 1813-1826.

10
11 11. Kalil, A.C., Patterson, T.F., Mehta, A.K., Tomashek, K.M., Wolfe, C.R., Ghazaryan, V.,
12 Marconi, V.C., Ruiz-Palacios, G.M., Hsieh, L., Kline, S., Tapson, V., Iovine, N.M., Jain,
13 M.K., Sweeney, D.A., El Sahly, H.M., Branche, A.R., Regalado Pineda, J., Lye, D.C.,
14 Sandkovsky, U., Luetkemeyer, A.F., Cohen, S.H., Finberg, R.W., Jackson, P.E.H., Taiwo, B.,
15 Paules, C.I., Arguinchona, H., Erdmann, N., Ahuja, N., Frank, M., Oh, M.D., Kim, E.S.,
16 Tan, S.Y., Mularski, R.A., Nielsen, H., Ponce, P.O., Taylor, B.S., Larson, L., Roupheal, N.G.,
17 Saklawi, Y., Cantos, V.D., Ko, E.R., Engemann, J.J., Amin, A.N., Watanabe, M., Billings, J.,
18 Elie, M.C., Davey, R.T., Burgess, T.H., Ferreira, J., Green, M., Makowski, M., Cardoso, A.,
19 de Bono, S., Bonnett, T., Proschan, M., Deye, G.A., Dempsey, W., Nayak, S.U., Dodd, L.E.,
20 Beigel, J.H., ACTT-2 Study Group Members. Baricitinib plus Remdesivir for Hospitalized
21 Adults with Covid-19. *N. Engl. J. Med.* **2021**, *384*, 795-807.

31
32 12. Cai, Qi., Yang, M., Liu, D., Chen, J., Shu, D., Xia, J., Liao, X., Gu, Y., Cai, Q., Yang, Y.,
33 Shen, C., Li, X., Peng, L., Huang, D., Zhang, J., Zhang, S., Wang, F., Liu, J., Chen, L., Chen,
34 S., Wang, Z., Zhang, Z., Cao, R., Zhong, W., Liu, Y., Liu, L. Experimental Treatment with
35 Favipiravir for COVID-19: An Open-Label Control Study. *Engineering (Beijing)*. **2020**, *6*,
36 1192-1198.

41
42 13. Sheahan, T. P., Sims, A. C., Zhou, S., Graham, R. L., Pruijssers, A. J., Agostini, M. L.,
43 Leist, S. R., Schäfer, A., Dinno III, K. H., Stevens, L. J., Chappell, J. D., Lu, X., Hughes, T.
44 M., George, A. S., Hill, C. S., Montgomery, S. A., Brown, A. J., Bluemling, G. R., Natchus,
45 M. G., Saindane, M., Kolykhalov, A. A., Painter, G., Harcourt, J., Tamin, A., Thornburg, N.
46 J., Swanstrom, R., Denison, M. R., Baric, R. S. An orally bioavailable broad-spectrum
47 antiviral inhibits SARS-CoV-2 in human airway epithelial cell cultures and multiple
48 coronaviruses in mice. *Sci. Transl. Med.* **2020**, *12*, eabb5883.

- 1
2
3 14. World Health Organization. WHO discontinues hydroxychloroquine and
4 lopinavir/ritonavir treatment arms for COVID-19. Available on-line at:
5 [https://www.who.int/news-room/detail/04-07-2020-who-discontinues-](https://www.who.int/news-room/detail/04-07-2020-who-discontinues-hydroxychloroquine-and-lopinavir-ritonavir-treatment-arms-for-covid-19)
6 [hydroxychloroquine-and-lopinavir-ritonavir-treatment-arms-for-covid-19](https://www.who.int/news-room/detail/04-07-2020-who-discontinues-hydroxychloroquine-and-lopinavir-ritonavir-treatment-arms-for-covid-19) (accessed on
7 July 18th, 2020).
8
9
10
11
12
13 15. Cavalcanti, A.B., Zampieri, F.G., Rosa, R.G., Azevedo, L.C.P., Veiga, V.C., Avezum, A.,
14 Damiani, L.P., Marcadenti, A., Kawano-Dourado, L., Lisboa, T., Junqueira, D.L.M., de
15 Barros e Silva, P.G.M., Tramujas, L., Abreu-Silva, E.O., Laranjeira, L.N., Soares, A.T.,
16 Echenique, L.S., Pereira, A.J., Freitas, F.G.R., Gebara, O.C.E., Dantas, V.C.S., Furtado,
17 R.H.M., Milan, E.P., Golin, N.A., Cardoso, F.F., Maia, I.S., Hoffmann Filho, C.R., Kormann,
18 A.P.M., Amazonas, R.B., Bocchi de Oliveira, M.F., Serpa-Neto, A., Falavigna, M., Lopes,
19 R.D., Machado, F.R., Berwanger, O. Hydroxychloroquine with or without Azithromycin in
20 Mild-to-Moderate Covid-19. *N. Eng. J. Med.* **2020**, *383*, 2041-2052
21
22
23
24
25
26
27
28
29 16. Horby, P., Lim, W. S., Emberson, J. R., Mafham, M., Bell, J. L., Linsell, L., Staplin, N.,
30 Brightling, C., Ustianowski, A., Elmahi, E., Prudon, B., Green, C., Felton, T., Chadwick, D.,
31 Rege, K., Fegan, C., Chappell, L. C., Faust, S. N., Jaki, T., Jeffery, K., Montgomery, A.,
32 Rowan, K., Juszczak, E., Baillie, J. K., Haynes, R., Landray, M. J. Dexamethasone in
33 Hospitalized Patients with Covid-19 — Preliminary Report. *N. Engl. J. Med.* **2021**, *384*, 693-
34 704.
35
36
37
38
39
40
41 17. Anand, K., Ziebuhr, J., Wadhwani, P., Mesters, J. R.; Hilgenfeld, R. Coronavirus main
42 proteinase (3CLpro) structure: basis for design of anti-SARS drugs. *Science.* **2003**, *300*,
43 1763–1767.
44
45
46
47 18. Zhang, L., Lin, D., Sun, X., Curth, U., Drosten, C., Sauerhering, L., Becker, S., Rox, K.,
48 Hilgenfeld, Rolf. Crystal structure of SARS-CoV-2 main protease provides a basis for
49 design of improved α -ketoamide inhibitors. *Science.* **2020**, *368*, 409-412.
50
51
52
53
54 19. Dai, W., Zhang, B., Jiang, X.-M., Su, H., Li, J., Zhao, Y., Xie, X., Jin, Z., Peng, J., Liu, F.,
55 Li, C., Li, Y., Bai, F., Wang, H., Cheng, X., Cen, X., Hu, S., Yang, X., Wang, J., Liu, X., Xiao,
56
57
58
59
60

1
2
3 G., Jiang, H., Rao, Z., Zhang, L.-K., Xu, Y., Yang, H., Liu, Hong. Structure-based design of
4 antiviral drug candidates targeting the SARS-CoV-2 main protease. *Science*. **2020**, *368*,
5 1331-1335.
6
7

8
9 20. Jin, Z., Du, X., Xu, Y., Deng, Y., Liu, M., Zhao, Y., Zhang, B., Li, X., Zhang, L., Peng, C.,
10 Duan, Y., Yu, J., Wang, L., Yang, K., Liu, F., Jiang, R., Yang, X., You, T., Liu, X., Yang, X.,
11 Bai, F., Liu, H., Liu, X., Guddat, L. W., Xu, W., Xiao, G., Qin, C., Shi, Z., Jiang, H., Rao, Z.,
12 Yang, H. Structure of Mpro from COVID-19 virus and discovery of its inhibitors. *Nature*.
13 **2020**, *582*, 289-293.
14
15
16
17
18

19
20 21. Newman, D. J., Cragg, G. M. Natural Products as Sources of New Drugs over the Last
21 25 Years. *J. Nat. Prod.* **2007**, *70*, 461-477.
22
23

24 22. Mani, J. S., Johnson, J. B., Steel, J. C., Broszczak, D. A., Neilsen, P. M., Walsh, K. B.,
25 Naiker, M. Natural product-derived phytochemicals as potential agents against
26 coronaviruses: A review. *Virus Res.* **2020**, *284*, 197989.
27
28
29

30 23. da Silva Antonio, A., Silveira Moreira Wiedemann, L., Florencio Veiga-Junior, V.
31 Natural products' role against COVID-19. *RSC Adv.* **2020**, *10*, 23379–23393.
32
33
34

35 24. Wen, C.-C., Kuo, Y.-H., Jan, J.-T., Liang, P.-H., Wang, S.-Y., Liu, H.-G., Lee, C.-K.,
36 Chang, X S.-T., Kuo, C.-J., Lee, S.-S., Hou, C.-C., Hsiao, P.-W., Chien, S.-C., Shyur, L.-F.,
37 Yang, N.-S. Specific Plant Terpenoids and Lignoids Possess Potent Antiviral Activities
38 against Severe Acute Respiratory Syndrome Coronavirus. *J. Med. Chem.* **2007**, *50*, 4087-
39 4095
40
41
42
43
44

45 25. Jo, S., Kim, S., Shin, D. H., Kim, M.-S. Inhibition of SARS-CoV 3CL protease by
46 flavonoids. *J. Enzym. Inh. Med. Chem.* **2020**, *35*, 145–151.
47
48
49

50 26. Scior, T., Bender, A., Tresadern, G., Medina-Franco, J.L., Martínez-Mayorga, K., Langer,
51 T., Cuanalo-Contreras, K., Agrafiotis, D.K. Recognizing pitfalls in virtual screening: a
52 critical review. *J. Chem. Inf. Model.* **2012**, *52*, 867-881.
53
54
55
56
57

- 1
2
3 27. Santana, K., do Nascimento, L.D., Lima, E., Lima, A., Damasceno, V., Nahum, C.,
4 Braga, R.C., Lameira, J. Applications of Virtual Screening in Bioprospecting: Facts, Shifts,
5 and Perspectives to Explore the Chemo-Structural Diversity of Natural Products. *Front.*
6 *Chem.* **2021**, *9*, 662688.
7
8
9
10
11 28. Gupta, S., Singh, A. K., Kushwaha, P. P., Prajapati, K. S., Shuaib, M., Senapati, S.,
12 Kumar, S. Identification of potential natural inhibitors of SARS-CoV2 main protease by
13 molecular docking and simulation studies. *J. Biomol. Struct. Dyn.* **2020**. doi:
14 10.1080/07391102.2020.1776157
15
16
17
18
19 29. Kumara, A., Choudhirc, G., Shuklad, S. K., Sharmae, M., Tyagif, P., Bhushang, A.,
20 Rathore, M. Identification of phytochemical inhibitors against main protease of COVID-19
21 using molecular modeling approaches. *J. Biomol. Struct. Dyn.* **2020**. doi:
22 10.1080/07391102.2020.1772112
23
24
25
26
27 30. Gurung, A. B., Ali, M. A., Lee, J., Farah, M. A., Al-Anazi, K. M. Unravelling lead
28 antiviral phytochemicals for the inhibition of SARS-CoV-2 Mpro enzyme through *in silico*
29 approach. *Life Sci.* **2020**, *255*, 117831.
30
31
32
33 31. Feixas, F., Lindert, S., Sinko, W., McCammon, J. A. Exploring the Role of Receptor
34 Flexibility in Structure-Based Drug Discovery. *Biophys. Chem.* **2014**, *186*, 31–45.
35
36
37
38 32. Bellera, C.L., Llanos, M., Gantner, M.E., Rodriguez, S., Gavernet, L., Comini, M., Talevi,
39 A. Can drug repurposing strategies be the solution to the COVID-19 crisis? *Expert Opin.*
40 *Drug Discov.* **2021**, *16*, 605-612.
41
42
43
44 33. Labute P. Protonate3D: Assignment of ionization states and hydrogen coordinates to
45 macromolecular structures. *Proteins.* **2009**, *75*, 187–205.
46
47
48
49 34. Molecular Operating Environment (MOE). Chemical Computing Group Inc. 1010
50 Sherbooke St. West Suite #910 Montreal QC Canada H3A 2R7.
51
52
53
54
55
56
57
58
59
60

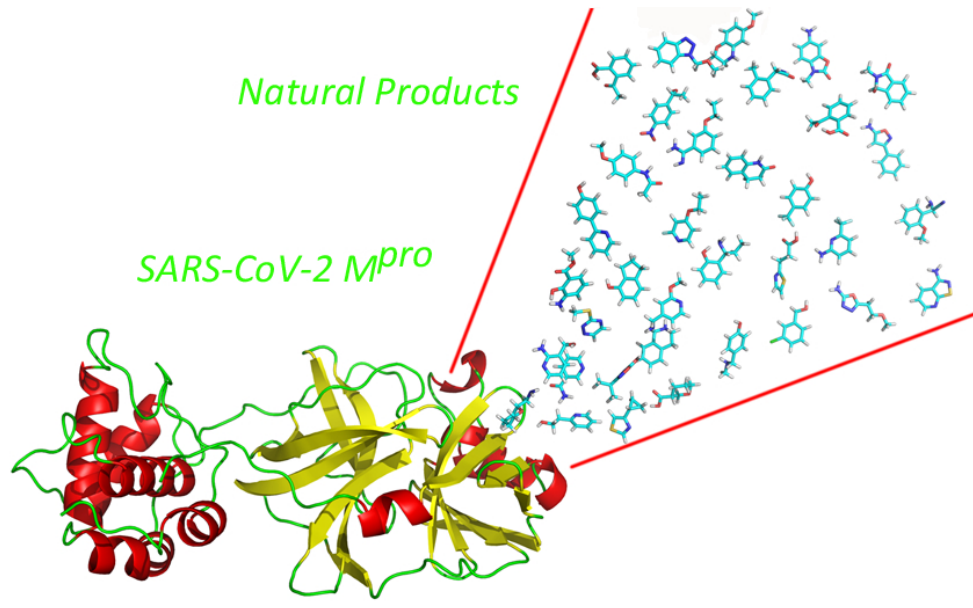
- 1
2
3 35. Izadi, S., Anandakrishnan, R., Onufriev, A. V. Building Water Models: A Different
4 Approach. *J. Phys. Chem. Lett.* **2014**, *5*, 3863–3871.
5
6
7
8 36. Case, D., Ben-Shalom, I. Y., Brozell, S. R., Cerutti, D. S., Cheatham III, T. E., Cruzeiro, V.
9 W. D., Darden, T., Duke, R. E., Ghoreishi, D., Gohlke, H., Goetz, A. W., Green, D., Harris,
10 R., Homeyer, N., Izadi, S., Kovalenko, A., Kurtzman, T., Lee, T. S., LeGrand, S., Li, P., Lin,
11 C., Luchko, T., Luo, R., Madej, B., Mermelstein, D. J., Merz, K. M., Miao, Y., Monard, G.,
12 Nguyen, H., Nguyen, H. T., Omelyan, I., Onufriev, A., Roe, D. R., Roitberg, A., Sagui, C.,
13 Schott-Verdugo, S., Shen, J., Simmerling, C., Smith, J., Salomon-Ferrer, R., Swails, J.,
14 Walker, R. C., Wang, J., Wolf, R. M., Wu, X., Xiao, L., York, D. M., Kollman, P. A., Amber
15 **2018**.
16
17
18
19
20
21
22
23 37. Tian, C., Kasavajhala, K., Belfon, K. A. A., Raguetta, L., Huang, H., Miguez, A. N.,
24 Bickel, J., Wang, Y., Pincay, J., Wu, Q., Simmerling, C. ff19SB: Amino-Acid-Specific Protein
25 Backbone Parameters Trained against Quantum Mechanics Energy Surfaces in Solution. *J.*
26 *Chem. Theory Comput.* **2020**, *16*, 528–552.
27
28
29
30
31 38. Darden, T., York, D., Pedersen, L. Particle mesh Ewald: An $N \cdot \log(N)$ method for Ewald
32 sums in large systems. *J. Chem. Phys.* **1993**, *98*, 10089.
33
34
35
36 39. Perez, J. J., Tomas, M. S., Rubio-Martinez, J. Assessment of the Sampling Performance
37 of Multiple-Copy Dynamics versus a Unique Trajectory. *J. Chem. Inf. Model.* **2016**, *56*,
38 1950-1962.
39
40
41
42 40. Roe, D. R., Cheatham T. E. PTRAJ and CPPTRAJ: Software for Processing and Analysis
43 of Molecular Dynamics Trajectory Data, *J. Chem. Theory Comput.*, **2013**, *9*, 3084-3095.
44
45
46
47 41. Rokach, L., Maimon, O. Data Mining and Knowledge Discovery Handbook, Maimon,
48 O., Rokach, L. Clustering Methods. Springer, pp. 321-352. Boston, MA, **2005**.
49
50
51 42. Amadei, A., Linssen, A. B., Berendsen, H. J. Essential Dynamics of Proteins, *Proteins*.
52 **1993**, *17*, 412-425.
53
54
55
56
57
58
59
60

- 1
2
3 43. Alhossary, A., Handoko, S. D., Mu, Y., Kwoh, C.-K. Fast, accurate, and reliable
4 molecular docking with QuickVina 2, *Bioinformatics*. **2015**, *31*, 2214–2216.
5
6
7
8 44. SelleckChem Natural Products Database.
9
10 <https://www.selleckchem.com/screening/natural-product-library.html> (accessed July, 18th
11 **2020**)
12
13
14 45. Wang, J., Wolf, R.M., Caldwell, J.W., Kollman, P.A., Case, D.A. Development and
15 testing of a general amber force field. *J. Comput. Chem.* **2004**, *25*, 1157–1174.
16
17
18 46. Jorgensen, W. L., Chandrasekhar, J., Madura, J. D. Comparison of simple potential
19 functions for simulating liquid water. *J. Chem. Phys.* **1983**, *79*, 926-935.
20
21
22
23 47. Maier, J. A., Martinez, C., Kasavajhala, K., Wickstrom, L., Hauser, K. E., Simmerling, C.
24 ff14SB: Improving the accuracy of protein side chain and backbone parameters from
25 ff99SB. *J. Chem. Theory Comput.* **2015**, *11*, 3696–3713.
26
27
28
29 48. Kuhn, B., Gerber, P., Shulz-Gasch, T., Stahl, M. Validation and Use of the MM-PBSA
30 Approach for Drug Discovery. *J. Med. Chem.* **2005**, *48*, 4040-4048.
31
32
33
34 49. Gohlke, H., Case, D. A. Converging Free Energy Estimates: MMPB(GB)SA Studies on
35 the Protein-Protein Complex Ras-Raf. *J. Comput. Chem.* **2004**, *25*, 238-250.
36
37
38
39 50. Kollman, P. A., Massova, I., Reyes, C., Kuhn, B., Huo, S., Chong, L., Lee, M., Lee, T.,
40 Duan, Y., Wang, W., Donini, O., Cieplak, P., Srinivasan, J., Case, D. A., Cheatham, T. E.
41 Calculating Structures and Free Energies of Complex Molecules: Combining Molecular
42 Mechanics and Continuum Models. *Acc. Chem. Res.* **2000**, *33*, 889-897.
43
44
45
46
47 51. Luo, R., David, L., Gilson, M. K. Accelerated Poisson-Boltzmann Calculations for Static
48 and Dynamic Systems. *J. Comput. Chem.* **2002**, *23*, 1244-1253.
49
50
51
52 52. Tsui, V., Case, D. A. Theory and Applications of the Generalized Born Solvation Model
53 in Macromolecular Simulations. *Biopolymers*. **2000**, *56*, 275-291.
54
55
56
57
58
59
60

- 1
2
3 53. Onufriev, A., Bashford, D., Case, D. A. Exploring Protein Native States and Large-Scale
4 Conformational Changes with a Modified Generalized Born Model. *Proteins*. **2004**, *55*, 383-
5 394.
6
7
8
9
10 54. Weiser, J., Shenkin, P. S., Still, W. C. Approximate Solvent-Accessible Surface Areas
11 from Tetrahedrally Directed Neighbour Densities. *Biopolymers*. **1999**, *50*, 373-380.
12
13
14 55. Miller, B. R., McGee, T. D., Swails, J. M., Homeyer, N., Gohlke, H., Roitberg, A. E.
15 MMPBSA.py: an Efficient Program for End-State Free Energy Calculations. *J. Chem.*
16 *Theory Comput.* **2012**, *8*, 3314–3321.
17
18
19
20 56. Lupala, C.L., Gomez-Gutierrez, P., Perez, J.J. New insights into the stereochemical
21 requirements of the bradykinin B2 receptor antagonist binding. *J. Comp.-Aided Mol.*
22 *Design*. **2016**, *30*, 85-101.
23
24
25
26
27 57. Krishna, S., Singh, D.K., Meena, S., Datta, D., Siddiqi, M.I., Banerjee, D.
28 Pharmacophore-Based Screening and Identification of Novel Human Ligase I Inhibitors
29 with Potential Anticancer Activity. *J. Chem. Inf. Model.* **2014**, *54*, 781–792.
30
31
32
33 58. Park, J., Park, R., Jang, M., Park, Y.-I. Therapeutic Potential of EGCG, a Green Tea
34 Polyphenol, for Treatment of Coronavirus Diseases. *Life*. **2021**, *11*, 197.
35
36
37
38 59. Du, A., Zheng, R., Disoma, C., Li, S., Chen, Z., Li, S., Liu, P., Zhou, Y., Shen, Y., Liu, S.,
39 Zhang, Y., Dong, Z., Yang, Q., Alsaadawe, M., Razzaq, A., Peng, Y., Chen, X., Hu, L., Peng,
40 J., Zhang, Q., Jiang, T., Mo, L., Li, S., Xia, Z. Epigallocatechin-3-gallate, an active ingredient
41 of Traditional Chinese Medicines, inhibits the 3CLpro activity of SARS-CoV-2. *Int. J. Biol.*
42 *Macromol.* **2021**, *176*, 1-12.
43
44
45
46
47
48 60. Jang, M., Park, R., Park, Y.I., Cha, Y.E., Yamamoto, A., Lee, J.I., Park, J. EGCG, a green
49 tea polyphenol, inhibits human coronavirus replication in vitro. *Biochem. Biophys. Res.*
50 *Commun.* **2021**, *547*, 23-28.
51
52
53
54
55
56
57
58
59
60

- 1
2
3 61. Jo, S., Kim, S., Shin, D.H., Kim, M.S. Inhibition of SARS-CoV 3CL protease by
4 flavonoids. *J. Enzyme Inhib. Med. Chem.* **2020**, *35*, 145-151.
5
6
7
8 62. Zhongren, X., Lixiang, Y., Xinghao, Z., Qiling, Z., Zhibin, Y., Yuanhao, L., Shuang, W.,
9 Wukun, L. Discovery of Potential Flavonoid Inhibitors Against COVID-19 3CL Proteinase
10 Based on Virtual Screening Strategy. *Front. Mol. Biosci.* **2020**, *7*, 556481.
11
12
13
14 63. Yoshino, R., Yasuo, N., Sekijima, M. Identification of key interactions between
15 SARS-CoV-2 main protease and inhibitor drug candidates. *Sci. Rep.* **2020**, *10*, 12493.
16
17
18
19 64. Mehany, T., Khalifa, I., Barakat, H., Althwab, S. A., Alharbi, Y. M., El-Sohaimy, S.
20 Polyphenols as promising biologically active substances for preventing SARS-CoV-2: A
21 review with research evidence and underlying mechanisms. *Food Bioscience.* **2021**, *40*.
22 100891.
23
24
25
26
27
28
29
30
31
32
33
34
35
36
37
38
39
40
41
42
43
44
45
46
47
48
49
50
51
52
53
54
55
56
57
58
59
60

1
2
3
4
5
6
7
8
9
10
11
12
13
14
15
16
17
18
19
20
21
22
23
24
25
26
27
28
29
30
31
32
33
34
35
36
37
38
39
40
41
42
43
44
45
46
47
48
49
50
51
52
53
54
55
56
57
58
59
60



TOC graphic

72x43mm (300 x 300 DPI)